Resilient yet entirely degradable gelatin-based biogels for soft robots and electronics.

Melanie Baumgartner[1,2,3]*, Florian Hartmann[1,2]*, Michael Drack[1,2], David Preninger[1,2], Daniela Wirthl[1,2], Robert Gerstmayr[2,3], Lukas Lehner[1,2], Guoyong Mao[1,2], Roland Pruckner[1,2], Stepan Demchyshyn[1,2], Lisa Reiter[1,2], Moritz Strobel[3], Thomas Stockinger[1,2], David Schiller[1,2], Susanne Kimeswenger[1,2,5], Florian Greibich[1,2], Gerda Buchberger[4,#], Elke Bradt[3], Sabine Hild[3], Siegfried Bauer[1,+] and Martin Kaltenbrunner[1,2,#]

[1]Division of Soft Matter Physics, Institute for Experimental Physics, Johannes Kepler University Linz, Altenberger Strasse 69, 4040 Linz, Austria

[2]Soft Materials Lab, Linz Institute of Technology, Johannes Kepler University Linz, Altenberger Strasse 69, 4040 Linz, Austria

[3]Institute of Polymer Science, Johannes Kepler University Linz, Altenberger Strasse 69, 4040 Linz, Austria

[4]Institute of Biomedical Mechatronics, Johannes Kepler University Linz, Altenberger Strasse 69, 4040 Linz, Austria

[5]Department of Dermatology and Venerology, Kepler University Hospital, Krankenhausstraße 7a, 4020 Linz, Austria

[#]correspondence: Martin Kaltenbrunner (MK), martin.kaltenbrunner@jku.at

*These authors contributed equally to this work

[#]Current affiliation: Institute of Applied Physics, Johannes Kepler University Linz, Altenberger Strasse 69, 4040 Linz, Austria

[+]deceased

Abstract:

Biodegradable and biocompatible elastic materials for soft robotics, tissue engineering or stretchable electronics with good mechanical properties, tunability, modifiability, or healing properties drive technological advance, yet they are not durable under ambient conditions nor combine all attributes in a single platform. We have developed a versatile gelatin-based biogel, which is highly resilient with outstanding elastic characteristics yet degrades fully when disposed. It self-adheres, is rapidly healable and derived entirely from natural and food-safe constituents. We merge for the first time all favorable attributes in one material that is easy to reproduce, scalable and low-cost in production under ambient conditions. This biogel is a step towards durable, life-like soft robotic and electronic systems that are sustainable and closely mimic their natural antetypes.

Main:

In 2025, an estimated 6 million tons of garbage will be generated per day[1], with tech disposables being a rapidly growing contributor. End-of-lifetime appliances contain valuable materials that are laborious in recovery or toxic substances that are readily released into nature through landfilling or improper treatment[2]. Biodegradable[3-6] and transient systems[7] are promising routes towards closing the loop on waste generation and create new opportunities for secure systems, but often at the cost of compromises in performance. Complex biological systems bridge this gap. They unite seemingly antagonistic properties - tough yet adaptive, durable and self-healing yet degradable - allowing them to perform a myriad of intricate tasks. Embodiments of technologies that intimately interface with humans naturally benefit from mimicking such soft, functional forms. A range of biomimetic systems[8] including soft machines[9] and electronic skins[10] achieve a high level of functionality by introducing self-healing[11,12], intrinsic stretchability[13], or the insightful merging of soft-to-hard materials[14]. Waste flow issues and in vivo applications that avoid multiple surgeries are tackled with inextensible devices in the form of edible[3,15] and transient electronics[7,16]. However, introducing stretchability to degradable devices remains challenging. Recent approaches focusing on stretchable biodegradable sensors[5] require expensive materials and are still wired to bulky measurement systems hindering implementation as wearable devices. Challenges here stem from the diverse material requirements,

ranging from mechanical resilience, durability and stretchability to high processability and low cost - while being entirely degradable. Synthetic materials such as polyester-based elastomers[17-20] or polyurethanes[21] degrade slowly and necessitate time and energy consuming synthesis, which may hamper their widespread market introduction. Bio-derived hydrogels[22-24] based on starch, alginate or collagen are cheap and offer fast degradation rates but typically fail to provide sufficient mechanical integrity under high loads. Strategies based on photo-crosslinking[25], inclusion of additional monomers[26,27], or salt treatment[28,29] help to overcome this issue but on the cost of processability, degradability, and price (Table 1).

Gelatin-based gels are a promising choice, since such biopolymers are readily derived without the need for synthesis, allow for water-soluble additives, are harmless to the environment due to fast degradation rates and even edible. Known to mankind for millennia, gelatin evolved from naturally derived glue to a widely used material in photographic films, food production, cosmetics and medications[30]. More recently, applications of gelatin span a diverse field from drug delivery[31], bone tissue engineering[32], including 3D printed scaffolds[33] and (micro)robotics[34] operating *in vivo*. Yet so far, gelatin-based gels have moderate performance when strained and rapidly dry when operated in air, which causes stiffening and limits stability and durability of wearable soft devices or soft robotic elements (Table 1, Supplementary Table 1, Supplementary Table 2). Existing examples of gelatin-based biodegradable soft actuators partially address these issues by maintaining a certain level of stretchability in the dried state[24], operating in salt-gradient electrolyte solutions[35], or using off the shelf confectionary gels[36]. However, all suffer from difficult to control material properties and limited stretchability leading to reduced performance of a few actuation cycles only.

We here introduce a fabrication approach, design rules, and a set of concepts for a broadly applicable gelatin-based biogel that for the first time unites the challenging needs of resilient yet sustainable (soft) robots and electronics in a single platform. Our gel is based on naturally occurring materials as degradable building blocks, durable, self-adhering, stretchable, mechanically tunable and healable. Despite being entirely degradable when disposed in wastewater, our gels maintain their mechanical

properties for more than one year under ambient conditions and enable soft actuators that operate for more than 330.000 cycles without failure. Scalable production, low material costs, and safety of all fabrication steps will enable widespread employment from industry and healthcare to education. Inspired by sophisticated living beings, from cephalopods to elephants, we combine our biogel with naturally derived materials, such as cellulose and zinc, to achieve fully biodegradable devices from robotic elements to stretchable electronics.

Cellulose as prevalent structural polysaccharide serves as textile exoskeleton for soft pneumatic biogel actuators (Fig. 1a) designed to operate in dynamic environments. Combining the biogel with structured zinc electrodes allows fully degradable sensor skins (Fig. 1b) paving the way for future biomedical devices that mimic our own skin. Our mechanically resilient biogel is an ideal material for temporary installations or frequently renewed applications that profit from transient devices as it breaks down into its building blocks within a few days (Fig. 1c, Supplementary Video 1, Supplementary Video 2) if triggered. They are cleaved enzymatically by wastewater bacteria within 5 days, rendering the biogel readily biodegradable according to standards of the Organisation for Economic Co-operation and Development (OECD) (Fig. 1d, Extended Data Fig. 1, see Supplementary Methods). Unlike simple dissolution that does not alleviate environmental concerns and may ultimately hamper *in vivo* applications through accumulation in filtration systems as the kidney[37], the more complete chemical degradation of individual polymer chains of gelatin enables disposal by the body and fully sustainable devices[38]. Where required, the dissolution onset of our biogels is significantly delayed in aqueous media and even in simulated stomach fluids using hydrophobic biodegradable coating strategies based on shellac resins (Supplementary Video 3, Methods). Coated biogels show no signs of dissolution after 48 h immersion in water or 24 h in acidic solution (pH 2.1). The degradation of the encapsulation layer is triggered in basic solutions (here pH 8.1), followed by complete dissolution of our biogel. This may open up routes for biodegradable applications underwater or *in vivo*.

We combine a variety of components – each serving a distinct purpose – to benefit from both biodegradation and high mechanical performance at the same time. Gelatin as main polymer network

of the gel defines the materials Young's modulus, the addition of sugars boosts extensibility. Stable mechanical properties and processing conditions are achieved by tuning the ratio of water and glycerol within the biogel, while citric acid prevents bacterial growth. Food grade additives introduce additional functionalities or structural properties without compromising the eco-friendliness and safety of the material (Supplementary Fig. 1). Detailed design rules that yield resilient and tough gels and compositions are in the Supplementary Discussion and Supplementary Table 3.

The wide range of emerging soft electromechanical systems - from electronic skins (e-skins) to robotics - demands a set of reliable and durable materials with readily tunable mechanical properties. We adjust the Young's modulus and the ultimate stress of our biogel by an order of magnitude (~30 kPa to ~300 kPa, ~10 kPa to ~140 kPa) by modifying the amount of gelatin, where both scale nearly exponentially with gelatin concentration (Fig. 2a, Supplementary Fig. 2a). Concurrently, the ultimate strain increases from 180 % to 325 % linear strain (Fig. 2b). Higher values of Young's modulus (3.1 MPa) are achieved by further increasing the gelatin concentration (Supplementary Fig. 2b), with improvements of ultimate stress (1.86 MPa) but a somewhat reduced ultimate strain (254 %). The high extensibility of our biogels is enabled by adding 28 wt% sugar syrup, increasing both tensile strength and ultimate strain (Fig. 2c & d, Supplementary Fig. 3a). The addition of sugars (and glycerol) as cosolvents drives biopolymer-biopolymer (helix-helix) association, enhances gelation and thermodynamically stabilizes gelatin gels[39], with an overall favorable impact on network formation. We hypothesize that unzipping of these helix-helix associations under high deformations leads to the observed increased extensibility. As a variety food-save additives interact with the gelatin network, we here achieve outstanding properties through meticulous and systematic optimization of all constituting materials.

Despite its high stretchability, our biogel shows a small hysteresis upon repeated cyclic stretching to 100 % linear strain with a constant energy dissipation after the second cycle of 6.4 kJ/m³ (Supplementary Fig. 4a, b). Limited fatigue sets in after thousands stretch-release cycles, yet no failure occurs after more than 100k cycles (Supplementary Fig. 5). Modifying the concentration of the base biopolymer provides a frugal route towards tuning the mechanical properties, likewise it

influences gelation, thermal stability and processability. Gelling time decreases from 12 min to 5 min, while gelling temperature increases from 39 °C to 50 °C by doubling the amount of gelatin, expanding its operational temperature range (Supplementary Fig. 6). Gelatin concentrations above 50 % complicate manual fabrication, but potentially provide stiffer material solutions in combination with advanced fabrication techniques such as injection molding or 3D printing.

Overcoming the drawback of water-rich polymers -- hydrogels which suffer from dehydration when used in ambient conditions owing to a loss of free water -- we replace large water fractions with the non-volatile food additive glycerol (a softener and humectant) to reduce the amount of free water in our biogel. A decreasing water-glycerol ratio extends the storage time and stability without influencing mechanical properties. Consequently, the dehydration related weight loss of the biogel is reduced from 25 % (G1620 formulation) to <5 % (G1644 formulation) when stored in ambient conditions for ~100 h (Fig. 2e) and remains below 10 % even in a very dry environment (23 °C, 20 %r.h., Supplementary Fig. 7). Additionally, increasing the glycerol concentration (from 20 wt% to 36 wt%) cancels unwanted material stiffening (Fig. 2f) and leads to nearly constant mechanical properties within 392 days storage time in ambient air (Fig. 2g). These modifications enable reliable stress-strain behavior and the fabrication of form-stable devices (Fig. 2h). No signs of material degradation are observed over the course of one year. We note that that these experiments were stopped due to time constraints only, suggesting that our biogels are stable for even longer time periods. Reducing the pH value of our biogels by the addition of citric acid prevents bacterial growth without influencing its stretchability (Fig. 2i, Supplementary Fig. 3b, Supplementary Fig. 8). Electing the constituent concentrations allows us to design an deformable and elastic biogel that does not dry out and is suitable for soft robotic applications operable within humidity ranges from 20 – 80 %r.h. (Supplementary Fig. 7, Supplementary Fig. 9). Biaxial stretching tests, performed by inflating a biogel disc into a balloon-shape (Fig. 2j, Supplementary Fig. 10, Supplementary Video 4), confirm areal strains beyond 1000 %. We model the strain distribution throughout the inflated balloon with the finite element method (FEM), showing a linear strain of 242 % at its apex (Fig. 2k), equivalent to over 1000 % areal strain (Fig. 2l). Even with a notch in the sample, the biogel withstands 109 J/m² before

crack propagation (Supplementary Fig. 11). Introducing biodegradable co-networks that potentially boost the gels fracture toughness may in future allow extremely soft yet tough biogels.

So far, soft robotic[40] and (wearable) healthcare applications[41] almost exclusively employ silicones or polyurethanes, which are barely degradable. While reliable high-performance materials are often a necessity, many tools from electrocardiography-electrodes to wound patches or endoscopy tubes are single use devices, operated for a short time. In addition, inherently safe and even edible elastic gels open up a cornucopia of applications from toys for children to robots that imitate other animals for behavior-studies or prey imitation[42].

Our biogel uniquely combines high performance and degradability, rendering it suitable for soft (bio-) robotics, medical appliances, and industrial robotic grippers disposed after their application. We here demonstrate the potential with a soft pneumatic actuator inspired by an elephant's trunk. The s-shaped movement of the pneumatically driven actuator reaches 10 cm maximum displacement of its tip (Fig. 3a). The actuator consists of a casted biogel-tube with a flexible air inlet and a textile exoskeleton made from crocheted cotton fibers, which direct the movement (Fig. 3b, Supplementary Fig. 12, Supplementary Fig. 13). We chose two pattern designs that result in s-shaped and u-shaped (simple bending) motion (Supplementary Fig. 14, Supplementary Video 5), imitating lift and grab movements of a trunk. The number of actuation cycles is monitored by inflating the u-shaped actuator with constant pressure against a plate connected to a force sensor. Actuators made from high water/glycerol ratio biogel (G2420) endure up to 10k cycles (ca. 10 h of constant actuation) and are promising for applications where intermediate durability is sufficient like customized rehabilitation actuators or rescue-robots that operate in hazardous environments. Actuators with lower water/glycerol ratio (G2430) are highly durable and show no failure even after 60k cycles. Here, the actuation force dropped to 40 % of the original value during the course of the experiments (2 days) due to some material fatigue (Supplementary Fig. 15). Using a force-regulated setup (adjusting the actuation pressure and frequency) boosts cycle lifetime to more than 330k cycles without failure (Fig. 3c, Supplementary Fig. 16), outperforming existing approaches by four orders of magnitude[24,36] and enabling integration of actuators or grippers in fabrication lines or as harvesting robots for otherwise

hand-picked produce[8,43,44]. Actuators operate for over 1.5 h and ~2k cycles even underwater when coated with edible oil (Supplementary Video 6). By constraining the movement of the tip, we show that they achieve a maximum force of 14.7 N at an applied pressure of 102 kPa (Supplementary Fig. 17).

Adding a biogel suction cup to the tube (connected to a vacuum pump) enables grasping and lifting diverse objects with flat or curved shapes up to 120 g for a distance of 16 mm (Fig. 3d, Supplementary Video 7). The u-shaped design enables bending angles of up to 286° (Fig. 3e), which corresponds to a maximum linear strain of 232 %, calculated from modelling the strain distribution of the actuator with FEM (Fig. 3f). The full range 281° bending angle is achieved by applying 50 kPa pressure (Fig. 3g). Discrete positions are reliably adjusted with an automated pressure control system (Supplementary Fig. 18). Additional functionalities, such as faunal defense mechanisms, are directly incorporated by adding fluorescent dyes. Such modified actuators glow in the dark under UV-illumination indicating the actuated state while the relaxed state appears dark due to the covering textile (Supplementary Fig. 19, Supplementary Video 5). The exoskeleton of our biogel actuator provides a platform that is easily manufactured with tools as simple as crocheting hooks and allows for fast prototyping of our safe kids-toy robot “Percy the Gellyfant” (Extended Data Fig. 2, Supplementary Video 8). Yet, it can readily be enhanced with biodegradable sensors to provide improved feedback and control. A biodegradable capacitive pressure sensor adds a tactile sense to our actuator and helps to recognize obstacles. We utilized the food additive mono- and diglycerides of fatty acids (E471) to create stable air bubbles within the biogel volume. Sandwiched between two zinc electrodes, this foam acts as a deformable capacitor (Fig. 3h, Supplementary Video 9) enabling the actuator to react to obstacles like a rose thorn. Applying a load compresses the voids in the soft foam (Fig. 3i) and approaches the two electrodes, resulting in an impedance change. We achieve a capacity change of factor 3 at repeated compression by a 100 kPa load (Fig. 3j). The slight hysteresis results from the foams mechanical response (Fig. 3k, Supplementary Fig. 4c, d), which exhibits larger energy dissipation compared to the incompressible biogel (G1620) due to the enclosed air voids.

Soft robots equipped with multimodal sensing capabilities provide the necessary environmental

feedback and will bring them a step closer to autonomy. One possible route to further improve robots is to implement soft e-skins[45] providing information about temperature, humidity or the state of deformation. The seamless integration of such e-skins on soft bodies is beneficial for robots and humans alike and may enhance wearable appliances from consumer electronics to medical diagnostic tools. However, the high throughput of medical appliances and their stringent hygiene requirements decrease their operational lifetime, raising demand on biodegradable solutions. Our biogel presents a self-adhering platform for biodegradable soft electronics that adheres to various surfaces without additional adhesives. We demonstrate autonomous sensor patches that are rapidly assembled from our tunable biogels by taking advantage of their thermoplastic properties.

Healing or assembly of the biogel is accomplished by brief local melting near a crack or cut with an infrared laser (Fig. 4a). Laser-healing of previously dissected biogels essentially fully restores their original mechanical properties (Fig. 4b) within less than 10 minutes of process time. We use this laser assisted rapid healing (LARH) to assemble biogels with different Young's moduli (1.4 MPa, 0.4 MPa, 0.2 MPa) into graded modulus gels. Uniaxial stretching of such modulus graded biogels reduces the strain in the stiffest part by 90 % at an overall strain of 50 % (Fig. 4c). We modelled the strain distribution by FEM and analytical calculations, and find good agreement with experiments in both cases (Supplementary Fig. 20). Rapid assembly using LARH allows realizing complex 3D shapes like a trefoil knot (Fig. 4d), or tailored, sophisticated substrates for stretchable electronics. We manufactured a biodegradable, stretchable multimodal electronic skin with temperature, humidity, and strain sensors using our biogel (Fig. 4e, Extended Data Fig. 3, Supplementary Fig. 21, Supplementary Fig. 22). The sensors, structured from zinc foil or temperature sensitive paste, are addressed by zinc meanders stretchable to 50 % uniaxial strain without change in resistance while enduring more than 1000 cycles when stretched to 20 % (Extended Data Fig. 4a-c). The sensor-data is recorded, analyzed, and transmitted wirelessly utilizing a reusable flexible printed circuit board (PCB) unit mounted on the biogel. This PCB features multichannel-impedance recording, analog-digital converters, current sources, and Bluetooth communication on a single autonomous platform (Supplementary Fig. 21, Supplementary Fig. 23). We choose this cost-effective approach as the PCB is readily recycled while to date broadband wireless data communication such as Bluetooth is still elusive in degradable form

factors. Future research will focus on overcoming this bottleneck by implementing basic functionality using transient radio-frequency transistor technology.

The temperature sensor made from a mixture of carnauba wax and graphite powder shows nearly linear resistance response in a temperature range from 10 °C to 40 °C (Fig. 4f, Extended Data Fig. 4g & h). The humidity sensor, designed as an interdigital electrode, follows an exponential decrease in impedance with increasing relative humidity (Fig. 4g). The change in impedance spans more than two orders of magnitude, yet its response to mechanical deformation of the skin is negligible due to its strain-isolated design (Extended Data Fig. 4d-f). The high number of fingers in combination with the graded modulus biogel greatly reduces the strain on the humidity sensor. Reducing the number of fingers and increasing their spacing allows large displacement of the electrodes on a soft biogel and renders a strain sensor with linear response while showing no hysteresis under cyclic stretch (Fig. 4h, Extended Data Fig. 4i & j). The sensor skin monitors temperature variations in proximity to a hot cup (Fig. 4i), humidity changes induced by aspiration (Fig. 4j), or deformation of the skin (Fig. 4k). The intrinsically adhesive biogel adheres to various surfaces, as evidenced with 90° peel-tests (Fig. 4l, Extended Data Fig. 5). In particular, we show stable interfacing with human skin even under twisting or shaking, but in addition allow for removal of the sensor patch without skin irritation (Supplementary Video 10). The biogel adheres to human skin even under elevated movement during sports and while sweating (Extended Data Fig. 6a-f). No signs of skin irritation are visible after 7 hours of wear. Prolonged contact to skin does not alter the mechanical properties of our biogels, they remain constant even after 38 hours of cumulative wear time during 4 days of routine daily activities (Extended Data Fig. 6g-j). Non-sticky versions are achievable if covered with talcum powder (Supplementary Video 11). Highly stretchable films with sub-mm thickness are readily fabricated using doctor blading (Supplementary Video 12). Based on our concept of a capacitive biodegradable pressure sensor, we design a pressure sensitive e-skin array from a 1 mm thick biogel foam together with a 4 x 4 matrix of zinc foil electrodes with stretchable interconnects (Fig. 4m & n). The stretchable pressure sensor array is addressed and read out by the flexible PCB (Fig. 4o, Extended Data Fig. 7, Supplementary Video 13). Besides being able to quantify a load on a single specific

sensor, the pressure sensor array detects objects with complex shapes (Fig. 4p & q). When stored in ambient conditions our e-skins remain functional for over a year, with somewhat reduced performance due to a higher signal to noise ratio (Supplementary Fig. 24).

In summary, we here introduce a set of biodegradable, resilient materials for soft robotics, electronic skins, and healthcare that are healable, deformable, self-adhering and resistant to dehydration. We apply our materials approach to create a new set of durable biodegradable soft actuators and autonomous electronic platforms with multimodal sensing capabilities. Possible applications range from edible robotics, produce harvesting, or animal behavior studies to single-use scenarios in hazardous environments or medical settings where tools and healthcare devices are commonly disposed after their employment to fulfill hygiene requirements. Implantable electronics or robots that operate underwater for an extended period of time still require biodegradable coatings that are hydrophobic, soft and at the same time stretchable. Our approach represents a frugal, environmentally benign and inexpensive route for future biodegradable technologies that avoid the incurrence of microplastics and are inherently safe when interacting with other lifeforms.

Methods

Methods and any associated references are available in the online version of the paper.

Data availability

All data needed to evaluate the conclusions in the paper are present in the paper and/or the Supplementary Information. All source files and experimental data are freely and publicly available at www.gel-sys.eu. Additional data related to this paper may be requested from the authors.

References

1. Hoornweg, D., Bhada-Tata, P. & Kennedy, C. Environment: Waste production must peak this century. *Nature* **502**, 615-617 (2013).

2. Leung, A., Luksemburg, W., Wong, A. & Wong, M. Spatial Distribution of Polybrominated Diphenyl Ethers and Polychlorinated Dibenzo-p-dioxins and Dibenzofurans in Soil and Combusted Residue at Guiyu, an Electronic Waste Recycling Site in Southeast China. *Environmental Science & Technology* **41**, 2730-2737 (2007).

3. Baumgartner, M. et al. Emerging "Green" Materials and Technologies for Electronics. in *Green Materials for Electronics.* 1–53 (Wiley-VCH: Weinheim, 2017)

4. Irimia-Vladu, M. et al. Biocompatible and Biodegradable Materials for Organic Field-Effect Transistors. *Advanced Functional Materials* **20**, 4069-4076 (2010).

5. Boutry, C. et al. A stretchable and biodegradable strain and pressure sensor for orthopaedic application. *Nature Electronics* **1(5)**, 314-321 (2018).

6. Walker, S. et al. Using an environmentally benign and degradable elastomer in soft robotics. *International Journal of Intelligent Robotics and Applications* **1**, 124-142 (2017).

7. Hwang, S. et al. A Physically Transient Form of Silicon Electronics. *Science* **337**, 1640-1644 (2012).

8. Yang, C. & Suo, Z. Hydrogel ionotronics. *Nature Reviews Materials* **3**, 125-142 (2018).

9. Acome, E. et al. Hydraulically amplified self-healing electrostatic actuators with muscle-like performance. *Science* **359**, 61-65 (2018).

10. Someya, T. & Amagai, M. Toward a new generation of smart skins. *Nature Biotechnology* **37**, 382-388 (2019).

11. Li, C. H. et al. A highly stretchable autonomous self-healing elastomer. *Nature chemistry* **6(8)**, 618 (2016).

12. Cao, Y. et al. Self-healing electronic skins for aquatic environments. *Nature Electronics* **2**, 75-82 (2019).

13. Wang, S. et al. Skin electronics from scalable fabrication of an intrinsically stretchable transistor array. *Nature* **555**, 83-88 (2018).

14. Wirthl, D. et al. Instant tough bonding of hydrogels for soft machines and electronics. *Science Advances* **3**, e1700053 (2017).

15. Wang, X. et al. Food-Materials-Based Edible Supercapacitors. *Advanced Materials Technologies* **1**, 1600059 (2016).

16. Bauer, S., Kaltenbrunner, M., Built to disappear. *ACS nano* **8(6)**, 5380-5382 (2014)

17. Yang, J., Webb, A. R. & Ameer, G. A. Novel citric acid-based biodegradable elastomers for tissue engineering. *Advanced Materials* **16**, 511–516 (2004).

18. Webb, A. R., Yang, J. & Ameer, G. A. Biodegradable polyester elastomers in tissue engineering. *Expert opinion on biological therapy* **4**, 801–812 (2004).

19. Wang, Y., Ameer, G. A., Sheppard, B. J. & Langer, R. A tough biodegradable elastomer. *Nature Biotechnology* **20**, 602–606 (2002).

20. Cohn, D. & Salomon, A. H. Designing biodegradable multiblock PCL/PLA thermoplastic elastomers. *Biomaterials* **26**, 2297–2305 (2005).

21. Skarja, G. A. & Woodhouse, K. A. In vitro degradation and erosion of degradable, segmented polyurethanes containing an amino acid-based chain extender. *Journal of Biomaterials Science, Polymer Edition* **12**, 851–873 (2001).

22. Averous, L., Moro, L., Dole, P. & Fringant, C. Properties of thermoplastic blends: starch–polycaprolactone. *Polymer* **41**, 4157–4167 (2000).

23. Zhu, C. et al. Highly stretchable HA/SA hydrogels for tissue engineering. *Journal of Biomaterials science, Polymer edition* **29**, 543–561 (2018).

24. Shintake, J., Sonar, H., Piskarev, E., Paik, J. & Floreano, D. Soft pneumatic gelatin actuator for edible robotics, *2017 IEEE/RSJ International Conference on Intelligent Robots and Systems (IROS)*, 6221-6226 (2017)

25. Van Den Bulcke, A. I. et al. Structural and rheological properties of methacrylamide modified gelatin hydrogels. *Biomacromolecules* **1**, 31–38 (2000).

26. Wu, T. et al. A ph-responsive biodegradable high-strength hydrogel as potential gastric resident filler. *Macromolecular Materials and Engineering* **303**, 1800290 (2018).

27. Ceseracciu, L., Heredia-Guerrero, J. A., Dante, S., Athanassiou, A. & Bayer, I. S. Robust and biodegradable elastomers based on corn starch and polydimethylsiloxane (PDMS). *ACS applied materials & interfaces* **7**, 3742–3753 (2015).

28. He, Q., Huang, Y. & Wang, S. Hofmeister effect-assisted one step fabrication of ductile and strong gelatin hydrogels. *Advanced Functional Materials* **28**, 1705069 (2018).

29. Qin, Z. et al. Freezing-Tolerant Supramolecular Organohydrogel with High Toughness, Thermoplasticity, and Healable and Adhesive Properties. *ACS Appl. Mater. Interfaces* **11**, 21184-21193 (2019).

30. Schrieber, R. & Gareis, H. *Gelatine Handbook.* (Wiley-VCH, Weinheim, Germany, 2007).

31. Luo, Z. et al. Biodegradable Gelatin Methacryloyl Microneedles for Transdermal Drug Delivery. *Advanced Healthcare Materials* **8**, 1801054 (2018).

32. Echave, M. et al. Enzymatic crosslinked gelatin 3D scaffolds for bone tissue engineering. *International Journal of Pharmaceutics* **562**, 151-161 (2019).

33. Mandrycky, C. et al. 3D bioprinting for engineering complex tissues. *Biotechnology Advances* **34(4)**, 422-434 (2016).

34. Kim, D., Lee, H., Kwon, S., Choi, H. & Park, S. Magnetic nano-particles retrievable biodegradable hydrogel microrobot. *Sensors and Actuators B: Chemical* **289**, 65-77 (2019).

35. Chambers, L., Winfield, J., Ieropoulos, I. & Rossiter, J. Biodegradable and edible gelatine actuators for use as artificial muscles. *Proceedings SPIE* **9056**, 90560B (2014)

36. Sardesai, A. et al. Design and Characterization of Edible Soft Robotic Candy Actuators. *MRS Advances* **3**, 3003-3009 (2018).

37. Deng, Y., Zhang, Y., Lemos, B. & Ren, H. Tissue accumulation of microplastics in mice and biomarker responses suggest widespread health risks of exposure. *Scientific Reports* **7**, 46687 (2017).

38. Feig, V., Tran, H. & Bao, Z. Biodegradable Polymeric Materials in Degradable Electronic Devices. *ACS Central Science* **4**, 337-348 (2018).

39. Shimizu, S., Matubayasi, N. Gelation: The role of sugars and polyols on gelatin and agarose. *The Journal of Physical Chemistry B* **118(46)**, 13210-13216 (2014).

40. Polygerinos P. et al. Soft Robotics: Review of Fluid-Driven Intrinsically Soft Devices; Manufacturing, Sensing, Control, and Applications in Human-Robot Interaction. *Advanced Engineering Materials* **19(12)**, 1700016 (2017).

41. Amjadi, M., Kyung, K.-U., Park, I. & Sitti, M. Stretchable, skin-mountable, and wearable strain sensors and their potential applications: a review. *Advanced Functional Materials* **26**, 1678–1698 (2016)

42. Krause, J., Winfield, A. & Deneubourg, J. Interactive robots in experimental biology. *Trends in Ecology & Evolution* **26**, 369-375 (2011).

43. Bogue, R. Fruit picking robots: has their time come? *Ind. Rob.* (2020) doi:10.1108/IR-11-2019-0243.

44. Hohimer, C. J. et al. Design and field evaluation of a robotic apple harvesting system with a 3d-printed soft-robotic end-effector. *Trans. ASABE* (2019) doi:10.13031/trans.12986.

45. Hartmann, F., Drack, M. & Kaltenbrunner, M. Meant to merge: Fabrication of stretchy electronics for robotics. *Science Robotics* **3**, eaat9091 (2018).

Acknowledgements

This work was supported by the European Research Council Starting Grant 'GEL-SYS' under grant agreement no. 757931, the Austrian Research Promotion Agency GmbH (FFG) within the COMET-project TextileUX under grant agreement no. 865791 and through startup funding of the Linz Institute of Technology (LIT) 'Soft Electronics Laboratory' under grant no. LIT013144001SEL. M.B. received support from Borealis and the Borealis Social Scholarship, VDI and the Dr. Maria Schaumayer Stiftung. G.B. acknowledges financial support from the European Commission within the 'LiNaBioFluid' project within the scope of H2020-FETOPEN-2014-2015-RIA. We thank Ewald Gelatine Germany, especially Dr. Thomas Hilt, for material support and fruitful discussions. We dedicate this work to Siegfried Bauer.

Author contributions

M.B., S.B., M.K conceived the research project; M.B. developed the materials with input from G.B. and S.H.; F.H., M.B., M.D. designed the experiments; M.B., L.L., D.P., F.H., L.R. prepared the materials; F.H., M.B., D.W., L.R., L.L., F.G., M.S., E.B. conducted mechanical materials characterization; M.B., R.G., D.P. performed BOD and dissolution tests; S.D. recorded the scanning electron microscopy images; G.M., F.H. conducted the mechanical simulations and modelling; M.B., D.P., F.H., developed and characterized the soft actuator; F.H., R.P., M.D., T.S. developed and characterized the degradable sensor patches; R.P., D.S. developed the flex. PCB and software; S.K. performed bacterial growth tests; F.H., D.W., M.D., analyzed the data; M.K. gave input at all stages; F.H., M.B., M.D., D.W. and M.K. wrote the manuscript; all authors contributed to editing the manuscript. M.K. supervised the research.

Additional information

Supplementary information is available in the online version of the paper. Reprints and permissions information is available online at www.nature.com/reprints. Correspondence and requests for materials should be addressed to M.K. (martin.kaltenbrunner@jku.at).

Competing financial interests

The authors declare no financial and non-financial competing interests.

METHODS

Materials

All chemicals were used as received without further purification. Gelatin powder (Bloom Factor 260, Ewald-Gelatine GmbH, Germany) was used for the main gel network, sugar syrup containing 17 % dextrose, 13.5 % maltose, 12 % maltotriose, and 57.5 % oligo-/polysaccharides (Glucose Syrup 45°, Grafschafter Krautfabrik Josef Schmitz KG, Austria) as co-solvent, citric acid (Carl Roth GmbH + Co. KG, Germany) to adjust the pH-value, and glycerol (Rotipuran ≥ 99.5 %, Carl Roth GmbH + Co. KG, Germany) to increase the bound water content of the biogel. E471 (Mono- and diglycerides of fatty acids) powder (Breinbauer Rohstoffe, Germany) was used as a stabilizer for biogel foams, riboflavin (E101, R9504-25G, Sigma-Aldrich, USA) for fluorescent biogels. Pure *Aloe vera* plant extract (local pharmacy) was used as an additive for a wound-healing biogel. We colored biogels with food dyes (Online-Konditor Mark Bünger, Germany) for visualization. A composite of carnauba wax (local pharmacy) and graphite powder (Graphitan 7525, Ciba Specialty Chemicals Inc., Switzerland) served as a temperature sensitive resistor. Zinc foil sheets (50 µm thick, ZN000230, GoodFellow GmbH, Germany) served as base conductive material for the sensor skins. Dewaxed Schellac (A. F. Suter & Co Ltd, England) mixed with polyethylene glycol (PEG 400, Sigma-Aldrich, USA) was used as an isolation layer for parts of the stretchable conductors of the pressure sensor matrix (close to the connections to the logic board). Actuator casting molds were printed using acrylnitril-butadiene-styrol (ABS) filament and covered by a releasing agent consisting of carnauba wax (local pharmacy), beeswax (local pharmacy), olive oil (local grocery store) and lecithin dissolved in water (E322, Breinbauer Rohstoffe, Germany).

Biogel preparation

Citric acid (1 g) and glycerol (8 g) were dissolved in deionized water (8 g) and heated to 60 °C. Sugar syrup (7 g) was heated to 60 °C to reduce its viscosity and mixed to the presolution. After cooling to room temperature, gelatin powder (4 g) was added and allowed to soak for 1 hour. The mixture was heated in an oven at 70 °C for 1 hour and stirred in a planetary mixer (DAC 600.2 VAC-P, Hauschild Engineering, Germany) under vacuum (2350 rpm, 450 mbar) for 4 minutes to achieve a homogeneous

precursor, which is ready for molding. Gel recipes with varying compositions that are used here are listed in Supplementary Table 3.

Biogel foam: E471 powder was dissolved in deionized water (ratio 1:2) for two hours under vigorous stirring. The dissolved E471 (8 g) was mixed with the biogel presolution and gelatin powder (4 g) and let soak for 1 hour. The mixture was heated at 65 °C for 1.5 hours and mixed with a hand blender for 30 seconds at 5000 rpm, resulting in a microfoam, which was cast into acrylic glass molds.

Biogel thin films: The prepared warm liquid biogel was poured on a teflon plate and distributed via doctor blading. The films were let to dry for one hour, resulting in a thickness of 0.58 mm. Coating with talcum powder renders non-sticky films.

Biogels with biodegradable encapsulation: Shellac solution was prepared according to Luangtana *et al*[46]. Schellac (36 g) was dissolved in ethanol (100 g). PEG 400 (7.2 g) was added to the shellac solution and stirred for 10 minutes. G2430 biogel samples were dip-coated in the shellac solution four times, followed by 30 min heating at 50°C in an oven and a final heating at 70 °C for 1 min. We repeated this procedure to achieve a homogeneous encapsulation of ~ 200 µm thickness.

Degradation and aging experiments

Biochemical oxygen demand (BOD): Ready biodegradability of gelatin biogels was investigated by closed bottle tests according to the OECD guideline for testing of chemicals. The beginning and end of biodegradation, the aerobic decomposition of organic compounds is identified via the oxygen uptake. To perform the degradation an aerated, tempered and inoculated mineral medium was prepared and stored sheltered from light. To investigate the oxygen uptake, test substances of the blank medium, a reference solution (medium + sodium acetate) and a test solution (medium + test sample) were prepared (300 mL). For the non-invasive analysis of the oxygen amount in the solutions a phase fluorometer (Neofox-GT, Ocean Optics, USA) and oxygen sensor patches (RedEye, Ocean Optics, USA) were used. The BOD is calculated from the initial and actual mean amount of dissolved oxygen in the solution (see Supplementary Methods) and was measured in a daily interval until day 11 and in a two-day interval afterwards. All measurements were performed in a dark and tempered (20 °C) room.

Mineral medium preparation: Four stock solutions were prepared (see SI) and 6 mL of each stock solution taken and diluted with 6 L deionized (DI) water. To improve the preservability 6 drops of concentrated hydrochloric acid (HCL) were added. The mineral medium was stored for 24 h at 20 °C and subsequently inoculated with 0.3 mL secondary effluent of a sewage plant and aerated overnight.

Dehydration: Circular samples (20 mm diameter) were punched out of 2 mm thick gel sheets (G1620, G1636, G1644 and G1215f). The samples were placed on a needle tip tripod to ensure air circulation on the entire sample surface and put on an analytical balance (AEJ 200-4CM, Kern & Sohn GmbH, Germany) in the climate chamber with climate conditions (20 °C, 40 %r.h.). Additional drying experiments at very low humidity (23 °C, 20 %r.h.) were performed with the most drying resistant gel (G1644, Supplementary Fig. 7). Relative humidity and temperature inside the chamber and the weight of the gel sample were measured and logged once every minute.

Dissolution of biogels: Circular samples (20 mm diameter) were punched out of 2 mm thick gel sheets (G1620, G1215f) and placed in a DI-water-filled beaker. The dissolution at constant temperature of 23 °C was captured with a camera (Fig. 1c, Supplementary Video 1 and Supplementary Video 2). Biogels with encapsulation were prepared as described above and equally tested in DI-water, citric acid solutions (pH 2.1), and trisaminomethane buffer solutions (pH 8.1) (Supplementary Video 3).

Influence of biogels on microbial growth: Autoclaved agar is filled in sterile cell culture dishes. Bacterial cells (XL1-Blue Competent Cells, Stratagene) are grown overnight in autoclaved Lysogeny Broth (Sigma-Aldrich). 100 µl and 500 µl of the overnight culture are plated on agar plates. Gelatin samples (41.0 mg ± 8.0 mg) are placed on agar plates arranged in a circle. As a positive control, a circular piece of paper is soaked with 10x antibiotic/antimycotic (Sigma-Aldrich). The plates are incubated at 37 °C for 24 hours. The growth of the bacteria is analysed visually and recorded using a digital camera.

Mechanical characterization of biogels

We used 2 mm thick biogels for characterization. Standardized dumbbell-shaped samples (ISO527-2:1996(5A)) were punched out of biogel sheets for uniaxial tensile tests. All biogels were unpacked

from their molds one week after casting. All tests were performed in ambient air at room temperature if not mentioned otherwise.

Biaxial stretching and pV-diagrams: Squared biogel sheets (G1620, G2420, and G2820, side length 40 mm) were colored, mounted on a pressure vessel with a circular clamp (aperture 30 mm) and inflated with air until material failure. The volume of the inflated gel was calculated from its curvature obtained by video analysis. The pressure was measured with a sensor (JUMO dTrans-p30, Fulda, Germany).

Uniaxial tensile tests: Uniaxial tensile tests of biogels were performed with a custom-made tensiometer (stretching speed of 1.25 mm/s) inside a climate chamber (C -40/350, CTS Clima Temperatur Systeme GmbH, Austria) at constant climatic conditions (23 °C, 40 %r.h.). The applied force was measured with a force gauge (KM26z 100N, ME-Meßsysteme GmbH, Germany), while the elongation was read from the step-motor controller (TMCM-1111, Trinamic). Single Young's modulus values were calculated from a regression using the Neo-Hookian model for incompressible elastomers. Samples with varying amount of gelatin but unchanged quantity of all other constituents were tested (samples G(09-28)20). Influence of the glycerol concentration was tested by changing the ratio of water and glycerol whereby the total amount of water and glycerol was kept constant at 52 wt% (samples G16(20-44)). To test the influence of storage time, biogels (G1620 and G1636) were stored under ambient conditions. Cyclic tensile tests of biogels (G1620 and G1215f) were performed by stretching to 100 % ultimate strain for 5 cycles. The dissipated energy was calculated from the area between extension and relaxation curves.

Peel tests: We measured the debond energy between the G1644 biogel (120 mm x 30 mm x 1.5 mm) and diverse substrates polydimethylsiloxane (PDMS), Ecoflex, porcine skin, paper, aluminum; 35 mm x 75 mm) via a 90° peel test. The biogel was covered with a 6 µm thick polyethylene terephthalate (PET) foil after casting to prevent elongation of the biogel during peeling. The porcine skin was pre-treated by shaving and heating up to 37 °C mimicking body temperature.

Fabrication of the biogel actuators

Casting: Biogel (G2430) precursors were molded in 3D-printed preheated molds in a two-step casting process. First, we cast a semi-open tube that was removed from its mold after cooling. Second, we cast a few millimeter thin layer of precursor into the mold in which we inserted a silicone tube (1.65 mm outer and 0.76 mm inner diameter, Freudenberg Medical, Germany) and immediately inserted the semi-open tube into the precursor to close it (Supplementary Fig. 12).

Textile exoskeleton: The textile exoskeleton was crocheted with cotton yarn and designed to guide the motion of the biogel actuator. We fabricated two designs enabling a u-shaped and s-shaped motion, respectively. Both designs are based on a building block consisting of interconnected ribs that allow for deformation of the actuator tube and tightly connected meshes that constrain deformation.

Actuator assembly: The biogel actuator tube was inserted into the textile exoskeleton and the ribs are aligned in parallel. The rear end of the exoskeleton is sewed onto a connection plate, to fix the actuator in different setups. The elephant head is assembled from laser-cut plywood plates.

Fluorescent actuator and elephant: The actuator tube and elephants were cast from G2430r UV-fluorescent biogel and inserted into the s-shape exoskeleton. The actuator was inflated manually under UV-illumination (365 nm, 120m W/cm², LED-Spot 100 with LED Powerdrive 40, Dr. Hönle AG, Germany).

Actuator characterization

If not mentioned otherwise, all tests were performed on a u-shaped actuator from G2430 biogel under ambient conditions. The actuation stroke as a measure of actuator performance was measured with a force cell (KM26z 100 N, ME-Meßsysteme GmbH, Germany).

Pressure control unit: The pneumatics include a compressor (N86KN.18, KNF Neuberger SAS, France) connected to a regulating valve, a solenoid valve (VDW Series, SMC, Japan) and the actuator. A second solenoid valve serves as air outlet for the actuator. A microcontroller (Arduino UNO, Arduino S.r.l., Italy) operates the solenoid valves. The pressure is recorded using a pressure sensor (40PC Series, Honeywell, USA).

Bending angle: To test the bending angle, the actuator was fixed in vertical position and inflated using the pressure control unit until a full turn was achieved (Fig. 3e, Supplementary Fig. 18a).

Actuator simulation: We modelled the deformation field using the commercial finite element method (FEM) software ABAQUS/Standard (SIMULIA, Dassault Systemes) with a simplified model of the actuator.

Maximum force test: The actuator (133 mm length) was put into a polyvinyl chloride (PVC) tube (27 mm inner diameter, 90 mm length) to keep the tip positioned perpendicular to the force cell (Supplementary Fig. 17). This constraint minimizes nonlinear effects and keeps the force concentrated on the tip. The pressure was controlled manually.

Durability test: U-shaped actuator tubes were cast from G2420 and G2430 biogels and fixed in perpendicular position to the force cell. We repeatedly inflated the actuators with constant pressure supply until the actuators either failed or performance dropped to ~40 %. Testing was performed inside the climate chamber at constant conditions (23 °C, 40 %r.h.). We repeatedly inflated an u-shaped actuator made from G2430 biogel until a force threshold of 0.2 N was reached, to test cyclic actuation with a constant force setting. The base pressure was adjusted manually, if needed.

Step-wise actuation: We used the s-shaped actuator on the wooden elephant head for step-wise actuation. The pressure in the actuator was controlled by the maximum pressure and the inflation time. The inflation time was controlled by a microcontroller, switching the solenoid valves. One complete inflation- and deflation-ramp started with the opening of the inflation-valve for 1 second, followed by closing for 3 seconds (hold time) and then opens again for another second with 3 seconds hold time. For deflation the deflation-valve was opened for 1 second with 3 seconds hold time and again opened for 4 seconds. Then the program started again with the inflation steps.

Suction cup fabrication and lifting of objects: For the suction cup we printed a two-part mold with a silicone tube (1.65 mm outer and 0.76 mm inner diameter, Freudenberg Medical, Germany) inserted at its bottom and cast the suction cup from G2430 biogel. Vacuum was applied manually with a syringe.

Pressure sensor

Assembly: Biogel foam sheets (G1215f, 2 mm thickness) were cast and dried in ambient conditions for one week, reducing the thickness to ~1.2 mm. Disks (12 mm diameter) were punched out and circular zinc foil electrodes (10 mm diameter) were attached on both sides.

Characterization: The pressure sensor was mounted on a rigid plate in a compression tester (Zwick Roell Z005, 2.5 kN load cell) and pressed by a cylindrical indenter (10 mm diameter). We measured the impedance change using an impedance analyzer (4284A Precision LCR Meter, HP, 1 kHz, 1 V).

Scanning electron microscopy (SEM): Thin stripes of G1215f biogel foam were prepared, 10-15 nm of gold (Au, Oegussa, 99.99%) were thermally evaporated (0.1-0.3 nm s^{-1}, $1x10^{-6}$ mbar) for improved surface conductivity. Measurement was performed using a Zeiss 1540 XB CrossBeam SEM with acceleration voltage of 3 keV.

Pressure sensor on actuator: Circular zinc electrodes (2 mm diameter) were attached on both sides of a biogel foam disk (4 mm diameter). The pressure sensor was mounted on a u-shaped actuator using gold wires. We actuated the sensor equipped actuator against the thorn of a rose or a screwdriver and measured the signal change of the deforming sensor. Reaching a certain threshold triggers immediate relaxation of the actuator.

Read out of pressure sensor on actuator: The pressure sensor was connected to a function generator that provided a sine with 1 V amplitude, 2 kHz and 2.5 V offset. We included the pressure sensor in a voltage-divider circuit to measure the voltage drop due to a capacity change of the sensor.

Toy robot

Percy: We crocheted "Percy the Elephant" from a pattern designed by Meredith May (Mostly Stitchin' Crochet). We used our textile exoskeleton design for the trunk, together with a smaller actuator tube, connected to a silicone tube. The trunk was actuated manually using a syringe.

Laser assisted rapid healing (LARH) and rapid assembly

LARH: Biogel samples (2 mm thickness) were cut with a knife and placed with a cleavage of less than 1 mm. The area around the cut interfaces was irradiated with a CO_2 laser (Speedy300, Trotec Laser

GmbH, Austria) (10.6 µm) in engraving mode, causing the biogel to melt locally and heal. The engraving pattern was repeated 5 times to ensure full healing of the samples.

Tensile tests: Half of the dumbbell-shaped samples (G1620) were cut in the center perpendicular to the stretching direction and healed by the LARH method. Uniaxial tensile tests were performed on both pristine and healed samples.

Trefoil knot: Rectangular stripes of G3030, G2430, and G1730 biogels (5 mm x 30 mm) were cut from 2 mm thick sheets and colored green, blue, and orange respectively. The stripes were assembled in series, healed with the LARH method, arranged in the trefoil knot configuration, and healed again at the open ends.

Graded modulus gels: Rectangular stripes of G3030 (25 mm x 20 mm), G2430 (15 mm x 20 mm), and G1730 (25 mm x 20 mm) biogels were cut from 2 mm thick sheets and colored green, blue, and orange, respectively. The stripes were assembled in series and healed with the LARH method. The stripe was mounted in a uniaxial stretching device with 10 mm broad clamps, leaving three unconstrained segments of 15-17 mm length each. The sample was manually stretched to a maximum total strain of 50 %. We calculated the overall strain behavior analytically by linearizing the stress-strain relationship and applying rules for composite materials. FEM modelling of the deformation field was performed by simplifying the material behavior with the Neo-Hookean model.

Biodegradable sensors and hybrid e-skins

Sensor fabrication: The biodegradable sensors and conductors were fabricated on biogel stripes by structuring applied zinc foil with the laser-cutter and removing excess material. Stretchable conductors and humidity sensors were fabricated on G2430 biogel, strain sensors on G1730 biogel, and temperature sensors on G3030 biogel. For the temperature sensor, temperature sensitive wax at 80 °C was coated through a mask (5 mm x 3.4 mm) on the center of the sensor.

Sensor characterization: All sensors were characterized inside the climate chamber. Resistance changes of conductors and temperature sensors were recorded with a multimeter (Keithley Model 2000). Impedance changes of strain and humidity sensors were recorded with an impedance analyzer

(4284A Precision LCR Meter, HP, 1 kHz, 1 V). Uniaxial cyclic tensile tests were performed at 23 °C and 40 %r.h.

Flexible PCB and control units: The flexible PCB hosting all control, power, and communication electronics was designed and routed inhouse and externally fabricated (50 µm polyimide coated with 18 µm copper on top and bottom layer). All components were soldered onto the flexible PCB with standard solder (Sn60Pb39Cu1, RS Components).

Sensor patch assembly: Stripes from G3030 (green), G2430 (blue), and G1730 (orange) biogels were arranged and healed with the LARH method to form a patch with a graded Young's modulus (Extended Data Fig. 3). Zinc foil was placed on the patch and structured with a laser cutter. After peeling off the excess material, the temperature sensitive wax was coated onto the patch through a mask (5 mm x 7.5 mm and 5 mm x 4 mm) and the flexible PCB was soldered to the contacts of the e-skin.

Sensor patch characterization: The sensor patch was placed in the climate chamber and connected to a computer via the low-energy Bluetooth module. Climatic conditions were varied from 20 °C to 30 °C in temperature and 40 %r.h. to 60 %r.h. in humidity. The impedance (|Z|) from each sensor was logged at a frequency of 10 kHz for one minute in every climatic configuration, resulting in the sensors characteristics.

On-skin tests: The arm/hand shown in Fig. 4, Extended Data Fig. 6, and Supplementary Video S10 is that of M. B., who has given her permission to publish this media. We measured the temperature change of the e-skin in proximity to a cup filled with boiled water, the impedance changes due to a humidity change through aspiration, and the strain response due to deformation. The data was wirelessly transmitted to a computer via the Bluetooth module.

In a second test, the biogel adhesion to human skin was tested. Two samples of a G1730 biogel with a thickness of 1 mm and 2 mm and a diameter of 2 cm were prepared. To enhance adhesion, the biogel discs were moisturized before they were applied on the skin of the upper arm. The top side of the discs was covered with talcum powder to prevent sticking to the surrounding. The test started at 9am with normal daily activities, including a 30 minute walk outside 25-30 °C, ~50 %r.h.). The test person performed running for 30 minutes (13pm to 14pm) to show adhesion during sports activities.

Additionally, the test person exercised with dumbbells to increase the arm movement. The biogel was removed after 7 hours (Extended Data Fig. 6e, f).

In a third test, rectangular stripes (25 mm x 100 mm x 2 mm) of G1730 biogel were attached to the skin as described above. The samples were worn for 9, 16, 28, and 38 hours on skin (5-12 h each day) during normal daily activities. Dumbbell shaped samples were punched out of the stripes and characterized with tensile tests. The resulting mechanical properties were compared with reference samples of the same batches, which were stored at ambient conditions for the same time.

Touch sensor array: A sheet of biogel foam (G1215f, 67 mm x 105 mm x 1 mm) was partially coated with shellac to reduce crosstalk between stretchable conductors. Zinc foil was structured with the laser cutter, and gently pressed onto the foam under heat, leaving a 4 x 4 touch sensor array. The flexible PCB was soldered to the stretchable conductors. Touch signals were read out by impedance converters applying a signal of 80 kHz and wirelessly transmitted. We put cylindrical weights of 10 g, 20 g, and 50 g with diameters (12 mm, 15 mm, and 20 mm respectively) onto a single sensor, to test its performance. We successively put a 20 g weight onto four sensors of the array, to test single response of sensors. We placed a frame (21 mm inner side edge, 38 mm outer side edge) onto the touch sensor array, together with a 500 g weight as example for object detection.

References

46. Luangtana-anan, M., Nunthanid, J. & Limmatvapirat, S. Effect of molecular weight and concentration of polyethylene glycol on physicochemical properties and stability of shellac film. *Journal of agricultural and food chemistry* **58**, 12934–12940 (2010).

		Shelf life	Mechanics	Costs	Processability	Synthesis	Degradation
Polyesthers	POC[17,18]	n.a.	+	€€€	●●	+	> 6 m
	PGS[19]	n.a.	+	€€	●●	+	> 1.5 m
	PCL -co- PLA[20]	15 d	-	€€€	●●●	+	6 m - > 24 m
	Polyurethanes[21]	n.a.	+	€€€€	●●●	+	6 m - > 24 m
Hydrogels	PLS[22]	< 30 d	-	€€	●●●	-	< 10 d
	Starch/Silicone[27]	n.a	+	€€	●●	-	3 - 6 y
	HA hydrogel[23]	n.a.	-	€€€	●	-	2 m
	Gelatin/Glycerol[24]	n.a.	-	€	●●	-	< 10 d
	Gelatin/ammonium sulfate[28]	n.a.	+	€	●●	-	< 10 d
	GelMa[25]	< 6 m	-	€	●	+	< 10 d
	PVDT-GelMa[26]	n.a.	+	€€€€	●	+	< 10 d
	Gelatin biogel (This work)	> 13 m	+	€	●●●	-	< 10 d

Table 1 | Materials selection matrix for biodegradable elastomers. Selection of biodegradable elastomers and hydrogels that are possible candidates for soft robotics and electronics[17-28]. An expanded version and selection criteria are given in the supplementary information. Abbreviations: poly(1,8-octanediol citrate) (POC); poly(glycerol sebacate) (PGS); poly(ε-caprolactone) (PCL); poly(lactic acid) (PLA); plasticized starch (PLS); methacrylated gelatin (GelMa); poly(2-vinyl-4,6-diamino-1,3,5-triazine) (PVDT).

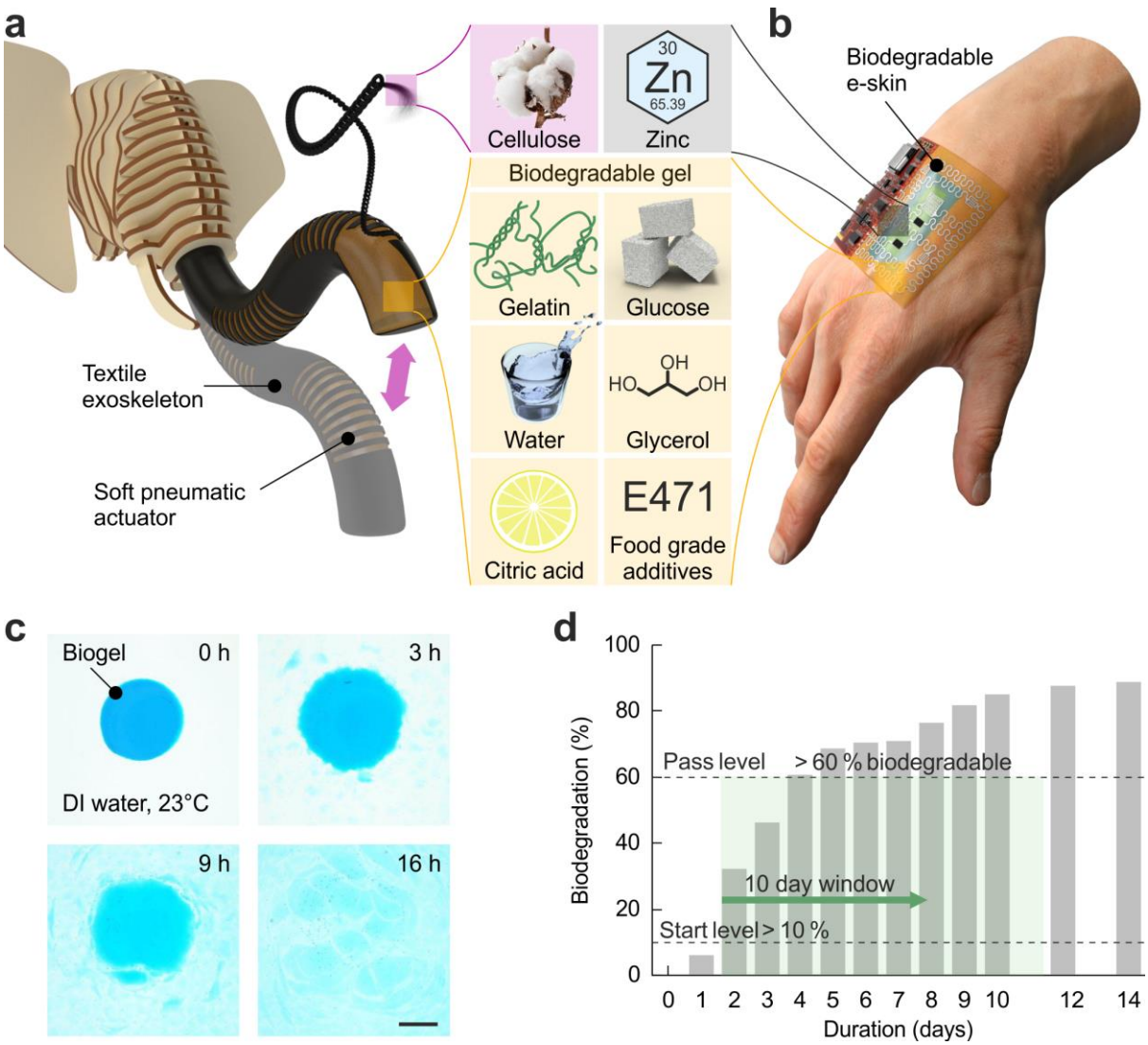

Figure 1 | A resilient yet fully degradable biogel. a & **b,** Naturally derived ingredients like gelatin and citric acid enable an elastic and stable, but fully degradable biogel. Together with cellulose fibers and zinc, soft and durable pneumatic actuators (a) and multifunctional electronic skins (b) are realized. **c**, Food-colored biogel disc immersed in deionized water dissolves within several hours. Scale bar, 1 cm. **d,** Complete aerobic decomposition of the biogel, measured via biological oxygen demand (BOD) of the microorganisms in the test solution (wastewater). The pass level for ready biodegradability is the removal of 60 % of dissolved organic compounds (DOC) in a 10 day window.

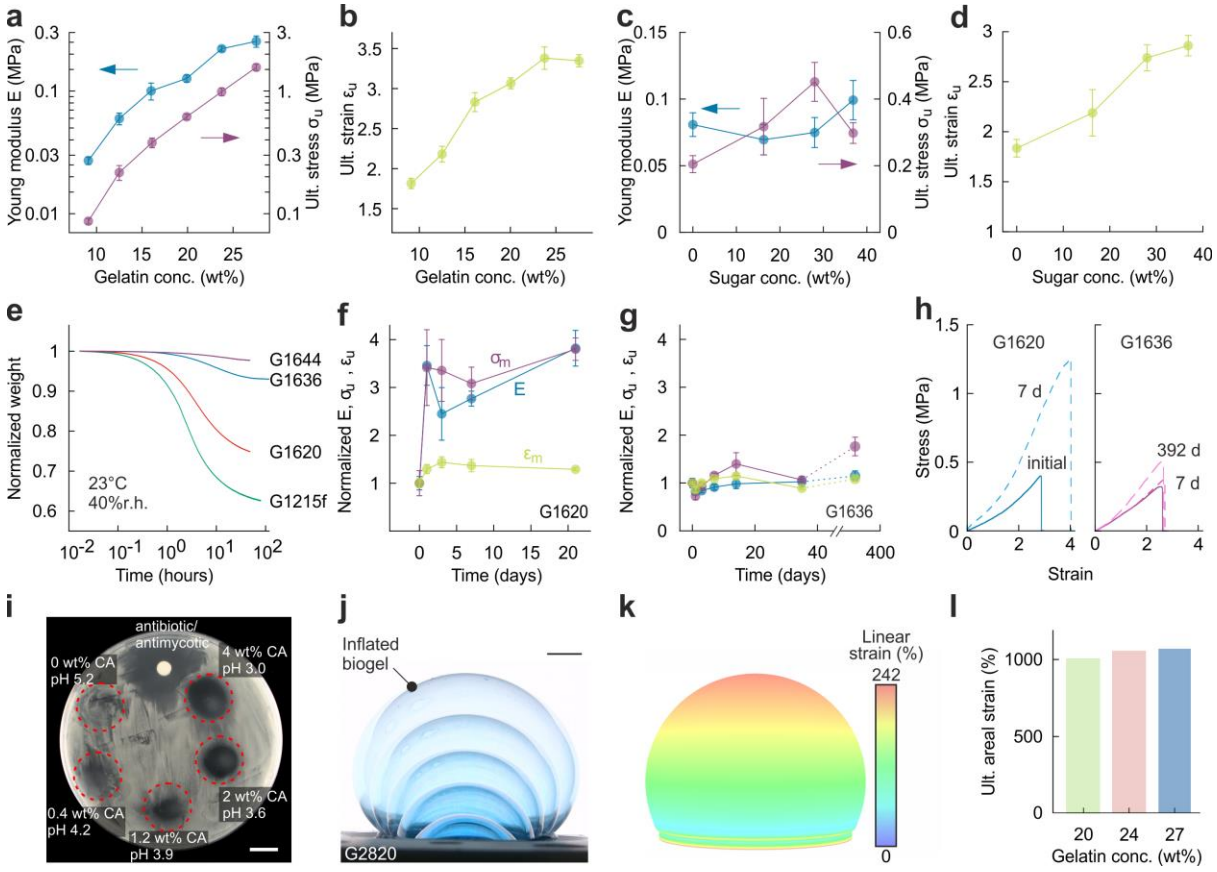

Figure 2 | Tunability, stability and extreme mechanics of gelatin biogels. a, The Young's modulus (E - blue) and the ultimate (engineering) stress (σ_u - purple) increase strongly with higher gelatin concentrations. **b,** The ultimate strain (ε_u - green) of dumbbell-shaped samples increases significantly for gelatin concentration up to 25 wt% and reaches saturation for higher values. **c,** Young's modulus (E) and ultimate stress (σ_u) as function of sugar concentration. While the Young's modulus changes only slightly, the ultimate stress maximizes at 28 wt%. **d,** Ultimate strain (ε_u) increases with sugar concentration, with only little changes above 28 wt%. **e,** Dehydration process of freshly prepared biogel samples of different water concentrations. **f,** Evolution of Young's modulus (E - blue), ultimate stress (σ_u - purple) and ultimate strain (ε_u - green) of a water-rich gel formulation (G1620). Within one day, E and ε_u increase by a factor of 3 whereas σ_u stays unaffected. **g,** Young's modulus (E - blue), ultimate stress (σ_u - purple) and ultimate strain (ε_u - green) of a low-moisture gel formulation (G1636) show no significant age-related changes when stored in ambient conditions for more than one year (392 days). **h,** Replacing parts of the water fraction with glycerol shows minor influence on the stress-strain behavior that otherwise quickly changes for water rich compositions. **i**, Increasing the citric acid

(CA) concentration prevents bacterial growth. Scale bar, 1 cm. **j**, Balloon-type inflation of a biogel membrane (G2820) in several actuation states. Scale bar, 1 cm. **k,** Mechanical simulation of an inflated biogel balloon. The maximum linear strain (longitudinal direction) is located at the apex of the balloon. **l,** Ultimate areal strain during balloon inflation of gels with varying gelatin concentration (G1620 green, G2420 red, G2820 blue). Error bars (a-d), standard deviation for n > 5 measurements. Error bars (f-g), standard deviation for n > 4 measurements.

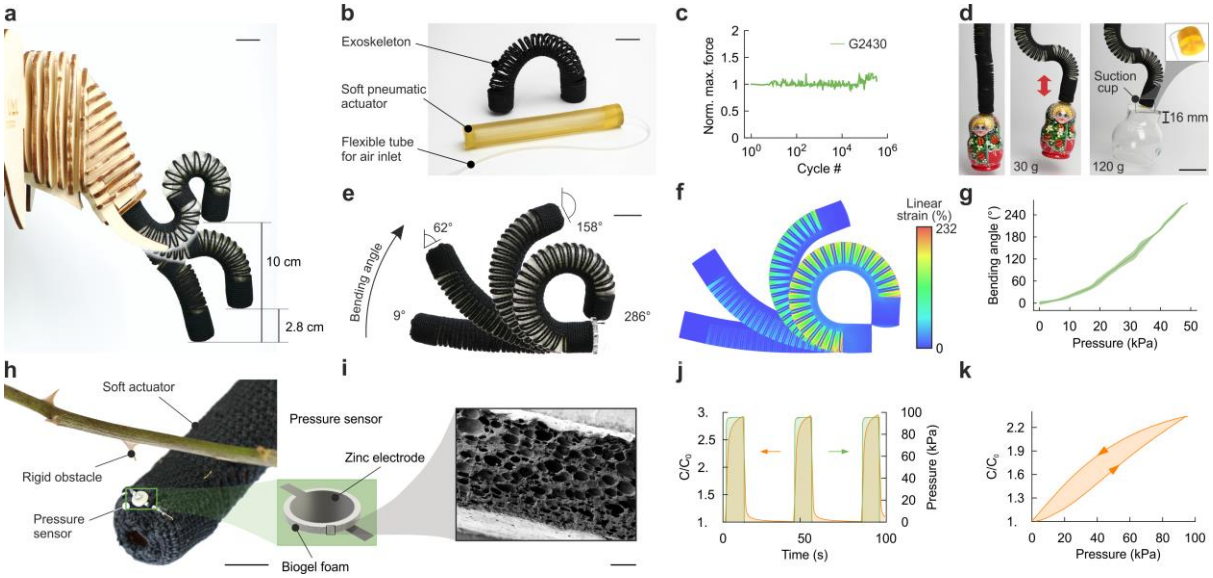

Figure 3 | Resilient biogels for soft actuators. a, Flexure of an s-shaped tube actuator. The fully deflected trunk achieves a displacement of 10 cm in vertical direction. Scale bar, 2 cm. **b,** Textile exoskeleton and inner gel tube of a soft pneumatic actuator. Scale bar, 2 cm. **c,** Cyclic actuation of a u-shaped actuator in ambient conditions. The actuator achieves over 330k cycles without failure in a force-regulated setup, using a low-moisture gel composition (G2430). **d,** A gel suction cup attached to the actuator (actuator weight ~35 g) allows lifting of variously shaped objects with a weight of up to 120 g. Scale bar, 4 cm. **e,** Several states of a u-shaped bending actuator. At the maximum angle bending is blocked by self-collision. Scale bar, 2 cm. **f,** Mechanical simulation of the u-shaped bending actuator. The linear strain is along the longitudinal direction of the actuator. **g,** The correlation between bending angle and applied pressure follows a linear behavior between 60° and the maximum angle. Mean (solid line) and standard deviation (shadow) for 4 consecutive measurements. **h,** Biodegradable pressure sensor on u-shaped actuator provides feedback from potential dangers like

a rose thorn. Scale bar, 1 cm. **i,** SEM picture of the biogel foam cross section. Scale bar, 200 µm. **j,** Pressure profile and responding capacity change of a pressure sensor. **k,** Characteristic for the pressure sensor showing a small hysteresis.

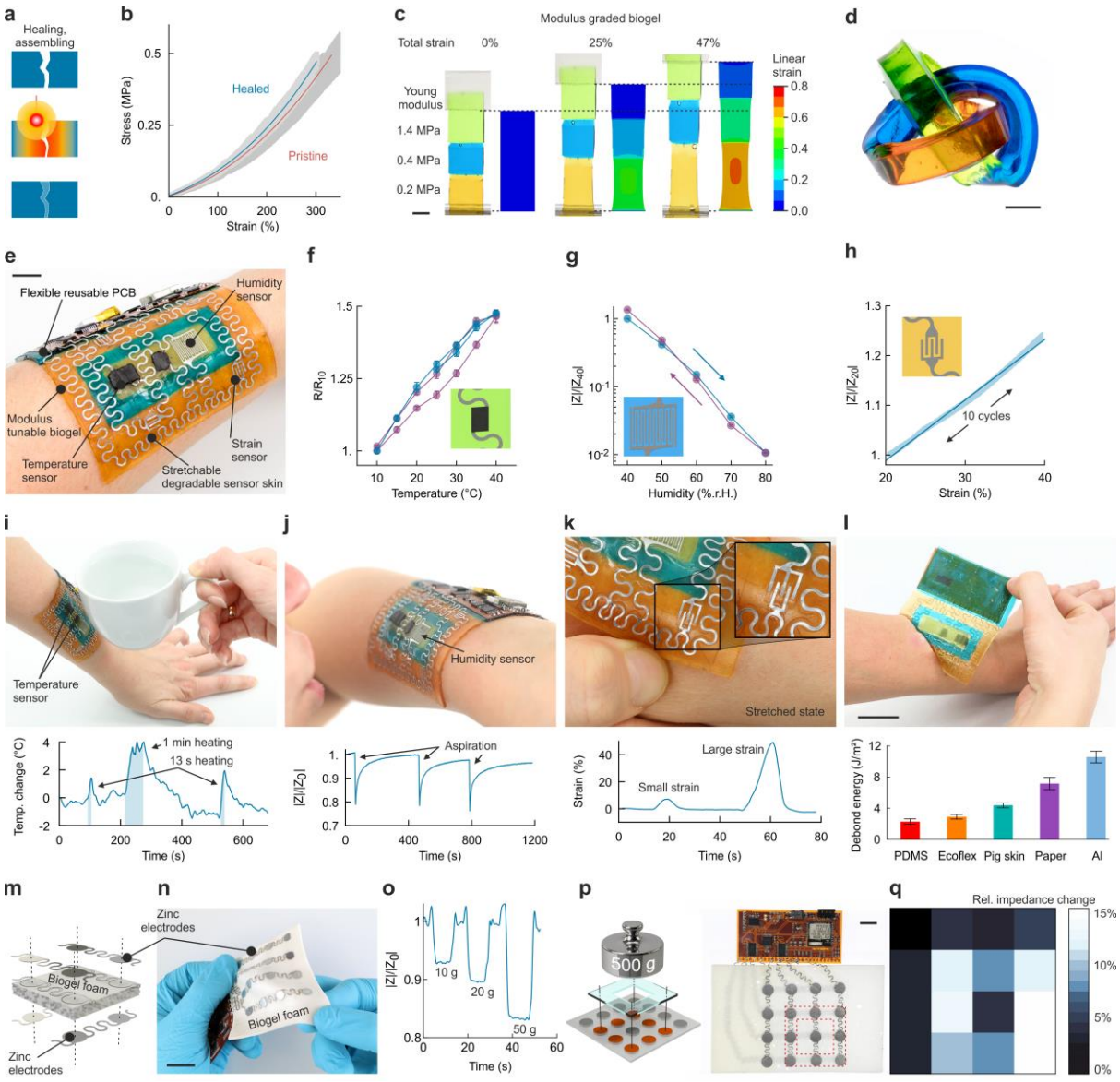

Figure 4 | Soft and degradable electronic sensor patches. a, Schematic of the laser assisted rapid healing (LARH) process. Edges to be joined are brought into near contact and selectively heated by a laser beam. A local liquefaction process allows a seamless bond. **b,** Stress-strain measurements of pristine and cut & healed gel samples (G1620) show no decrease in mechanical properties. Polynomial fit (solid line) and data envelope (gray shadow) for 7 individual samples each. **c,** Tensile test of a modulus graded gel compared with its FEM simulation. The strain is along the stretching

direction. Scale bar, 1 cm. **d,** A trefoil knot of three different gels (G1730, G2430, G3030) assembled by LARH. Scale bar, 5 mm. **e,** Soft electronic skin on a human arm. Scale bar, 3 cm. **f,** Characteristics of the biodegradable temperature sensor (G3030). The signal shows hysteresis during the third (purple) cycle, but it vanishes after the fourth (blue). Error bars, standard deviation for a measurement period >10 min. **g,** Characteristics of humidity sensor. Error bars, standard deviation for a measurement period >10 min. **h,** Performance of the strain sensor. Regression over 10 cycles demonstrates linear response. Linear fit (solid line) and data envelope (blue shadow) for 10 consecutive strain cycles. **i,** On-skin worn electronic patch is exposed to elevated temperatures (top). Exposures with different durations are recorded (bottom), **j,** Repeated aspiration onto the electronic patch (top) and resulting peaks in the humidity recordings (bottom). **k,** Mechanical deformation of strain sensors (top) and recordings for two different strain levels (bottom). **l,** Peel-off of the electronic patch (top). The debond energy was measured for G1644 on different substrates (bottom). Scale bar, 3 cm. Error bars, standard deviation for n > 3 measurements. **m,** Schematic showing orientation and design of zinc electrodes on biogel foam G1215f. **n,** Degradable stretchable pressure sensor array. Scale bar, 2 cm. **o,** Impedance response of a single pressure sensor impinged by different weights. **p,** Schematic and photograph of a 500 g weight distributed to a square shaped part of a 4x4 pressure sensor array. Scale bar, 1 cm. **q,** Signals recorded with the pressure sensor patch.

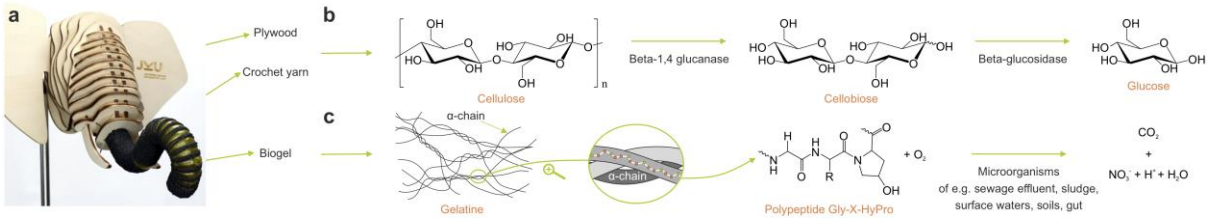

Extended Data Fig. 1 | Degradation of biomaterials. a, A bioinspired soft actuator consisting of wood, cotton-yarn, and gelatin-based biogel. **b,** Degradation reaction and end product of cellulose. **c,** Degradation and end product of gelatin. Single polypeptide strands are split by microorganisms found in waste water, gut, or soils.

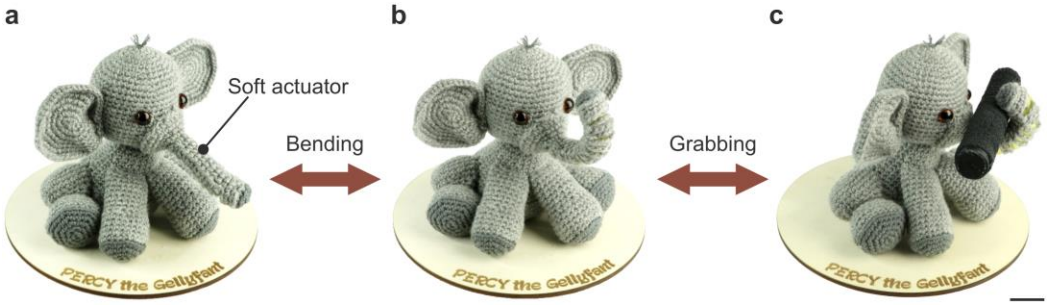

Extended Data Fig. 2 | Biodegradable soft robot demonstrator "Percy the Gellyfant". a, The manually actuated elephant trunk in its relaxed state and **b,** actuated u-shaped state. **c,** U-shaped movement allows grabbing of various objects. Scale bar, 2 cm.

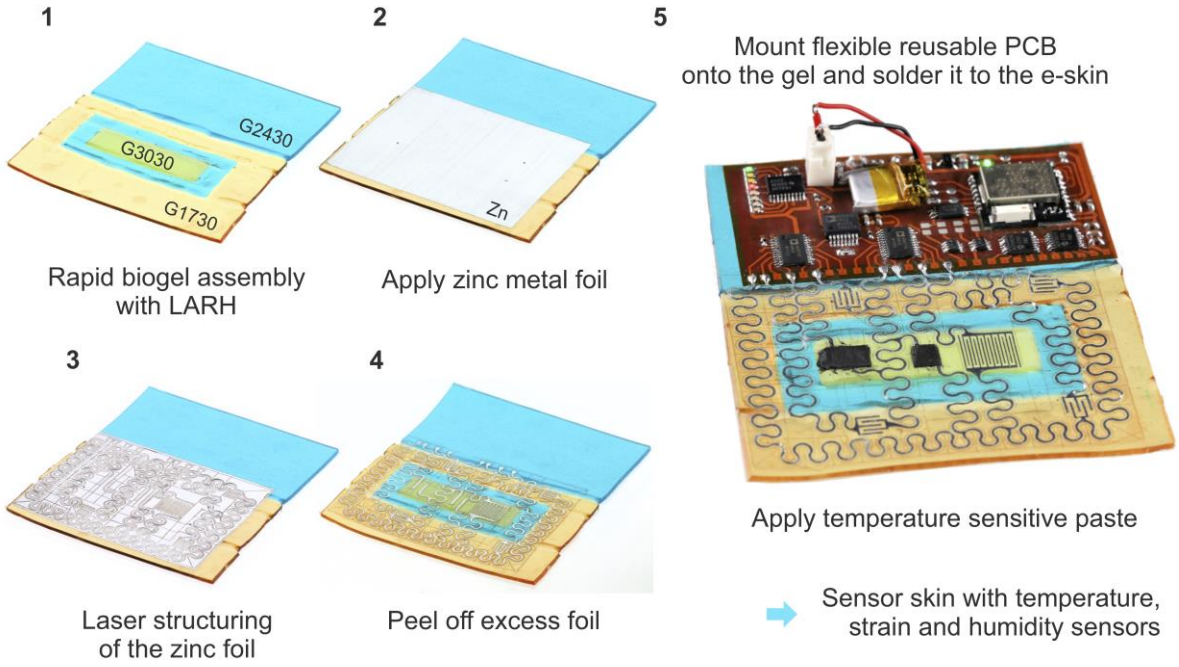

Extended Data Fig. 3 | Assembly of sensor skins. Assembly process of the sensor skin consisting of degradable e-skin and reusable PCB. **1,** Gels of different mechanical properties are joined by laser assisted rapid healing (LARH). **2-3,** A zinc metal sheet is then applied to the gel and structured by a fiber laser. **4,** After the structuring process the zinc residues are peeled off. **5,** A flexible reusable PCB is mounted on the gel and soldered to the zinc foil of the e-skin. In the last fabrication step a temperature sensitive paste is placed on the gel to finalize the temperature sensor.

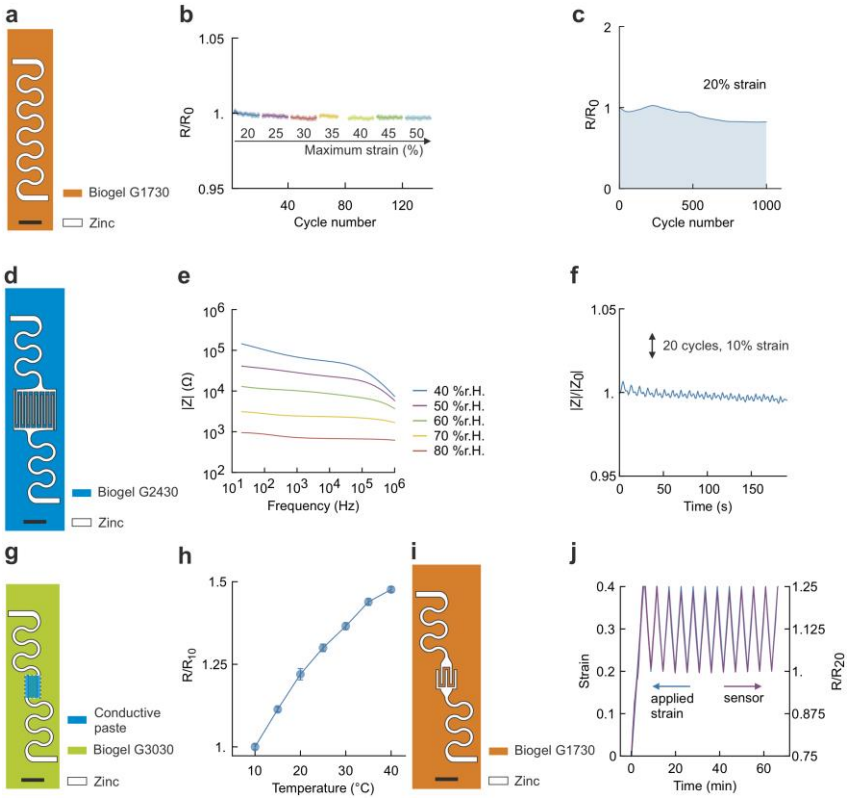

Extended Data Fig. 4 | Biodegradable sensors characterization. a, Stretchable meanders of zinc foil serve as conductors on biogels (G1730). **b,** Repeated stretching and increase of the maximum strain does not affect the conductivity of the zinc meanders. Mean resistance changes (solid line) during stretch-release cycles (data envelope) are shown. **c,** Those are durable for over 1000 stretching cycles, when stretched to a maximum strain of 20 %. **d,** Humidity sensors are realized with structured zinc foil on biogels (G2430). **e,** The magnitude of the impedance *Z* is measured as function of frequency at different climatic conditions, showing a change of two orders of magnitude. **f,** The sensor response is below 1 % when stretched repeatedly to a maximum strain of 10 %. **g,** Temperature

sensors are realized with a conductive paste between two stretchable conductors on a biogel (G3030). **h,** The conductive pastes, fabricated on glass substrates, show a change larger than a factor of 2 over a range of 30 °C. Error bars, standard deviation for a measurement period >10 min. **i,** Strain sensors are designed with 5 fingers total to allow displacement of the electrodes. **j,** The sensor signals follow the applied strain profile linearly. Repeated cycles are tested between 20 % and 40 % strain, to account for irreversible mechanical deformation of the substrate during the first stretch-release cycle. Scale bars, 5 mm.

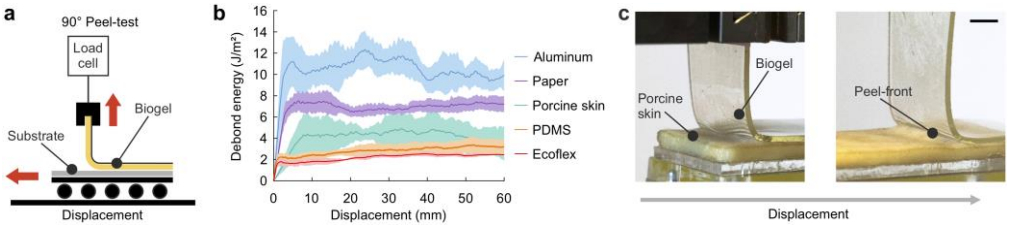

Extended Data Fig. 5 | Adhesion tests. a, Schematic of the 90° peel-test used to measure the debond energy between a biogel slightly pressed against diverse substrates. A 6 µm thick PET foil serves as stiff backing to prevent elongation of the peel arm, whereas a linear guiding ensures a constant angle of 90°. **b,** Measured debond energy for aluminum (blue), paper (purple), porcine skin (turquoise), PDMS (orange) and Ecoflex (red). **c,** Photographs of a biogel-porcine skin peel-sample taken during a peel-test showing the propagation of the peel-front between biogel and substrate. Mean values (solid line) and standard deviation (shadow) for n > 4 samples each. Scale bar, 1 cm.

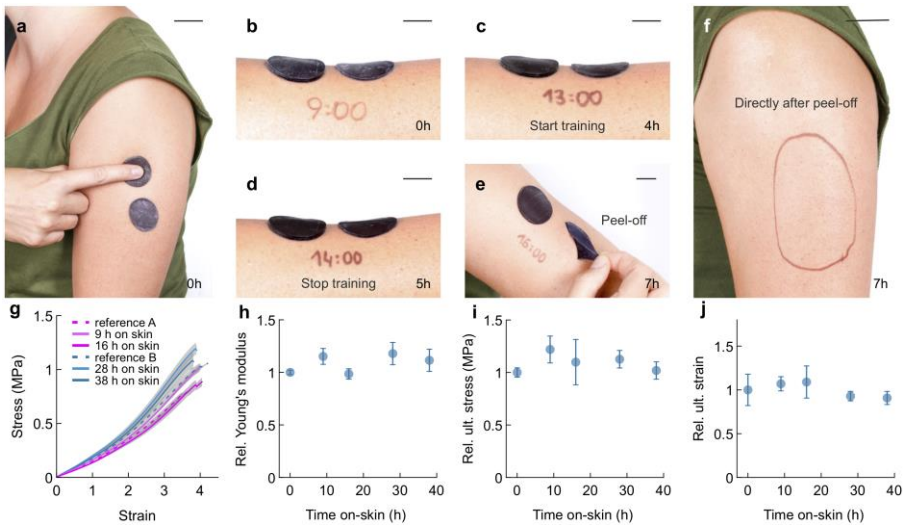

Extended Data Fig. 6 | On skin test - long time adherence. a, Two gel discs (G1730) with a thickness of 1 mm and 2 mm and a diameter of 2 cm were applied on the skin of the upper arm with little pressure. Scale bar, 2 cm. **b,** The test started at 9am, **c,** and showed no signs of gel disintegration during 4 hours of wearing. Scale bars, 1 cm. **d,** Even after sports activities (13pm to 14pm) that involved higher mechanical load and sweating, there are no signs of detachment. Scale bar, 1 cm. **e,** After 7 hours the biogel still adheres to the skin, even at the edges of the gel. Scale bar, 1 cm. **f,** The gel can be removed with no visible irritations after removal. Scale bar, 2 cm. **g,** Rectangular stripes were applied on the skin for up to 4 days (5-12 h each day) and compared to reference samples of the same batch. Mean values (solid line) and data envelope (gray shadow) for $n > 3$ samples each are shown. The biogel mechanics do not change upon wearing, even after 38 h wear-time on skin, resulting in constant **h,** Young's modulus (ref. A: 170 kPa ± 4 kPa, ref. B: 207 kPa ± 5 kPa), **i,** ultimate stress (ref. A: 830 kPa ± 60 kPa, ref. B: 1070 kPa ± 26 kPa), **j,** and ultimate strain (ref. A: 373 % ± 26 %, ref. B: 423 % ± 22 %). Error bars, standard deviation for a $n > 3$ measurements.

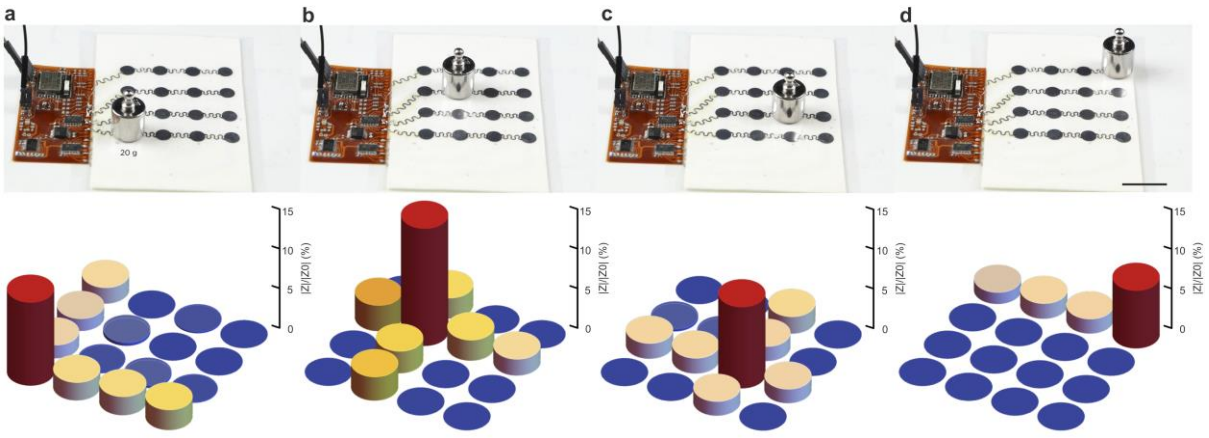

Extended Data Fig. 7 | Pressure skin. a-d, A weight of 20 g is applied to single pixels of the pressure skin sensor matrix. The measurement shows an impedance increase of 7-15 % compared to the initial value. Scale bar, 2 cm.